Screen-printed electrochemical immunosensor based on a novel nanobody for analyzing aflatoxin M1 in milk

Xiaoqian Tang, Gaëlle Catanante, Xiaorong Huang, Jean-Louis Marty, Hong Wang, Qi Zhang, Peiwu Li

Screen-printed electrochemical immunosensor based on a novel nanobody for analyzing aflatoxin M_1 in milk

Xiaoqian Tang [a,b,c,d,e,f], Gaëlle Catanante [f*], Xiaorong Huang [a], Jean-Louis Marty [g], Hong Wang [h], Qi Zhang [a,b,c*], Peiwu Li [a,b,c,d,e*]

[a] Oil Crops Research Institute, Chinese Academy of Agricultural Sciences, Wuhan, China

[b] Key Laboratory of Detection for Mycotoxins, Ministry of Agriculture and Rural Affairs, Wuhan, China

[c] Laboratory of Risk Assessment for Oilseeds Products, Ministry of Agriculture and Rural Affairs, Wuhan, China

[d] Key Laboratory of Biology and Genetic Improvement of Oil Crops, Ministry of Agriculture and Rural Affairs, Wuhan, China

[e] Quality Inspection and Test Center for Oilseeds Products, Ministry of Agriculture and Rural Affairs, Wuhan, China

[f] Laboratoire BAE-LBBM USR 3579, Université De Perpignan Via Domitia, 52 Avenue Paul Alduy, Perpignan Cedex 66860, France

[g] Sensbiotech, 21 rue de Nogarede , 66400 Ceret France

[h] Guangdong Provincial Key Laboratory of Food Quality and Safety, South China Agricultural University, Guangzhou 510642, PR China

Tel.: +86 86812862; +33 468662254

Fax: +86 86812862; +33 468662223

E-mail: gaelle.catanante@univ-perp.fr; zhangqi01@caas.cn; peiwuli@oilcrops.cn

Abstract

This study aimed to devise a nontoxic electrochemical immunosensor to quantitatively determine aflatoxin M_1 by chronoamperometry with novel anti-idiotypic nanobody-functionalized screen-printed carbon electrodes (SPCEs). Anti-idiotype nanobodies (AIdnb) were developed to replace the high toxic chemically synthesized antigen. AIdnb was immobilized on the surface of SPCE via covalent coupling as capture reagent. The functionalized SPCEs were followed by characterization using electrochemical impedance spectroscopy, fourier-transform infrared spectroscopy, transmission electron microscopy mapping, and atomic force microscopy. After optimizing experimental parameters, the assembled immunosensor exhibited a good linearity range of 0.25–5.0 ng/mL, with the limit of detection of 0.09 ng/mL. The immunosensor showed a satisfactory selectivity to AFM_1, without interference from analogs, including zearalenone, ochratoxin, and fumonisin B_1. For practical application, the developed immunosensor was validated using real spiked samples with the recovery range 82.0%–108.0% and relative standard deviation (RSD) 10.1%–13.0%, indicating that it could be used in milk samples.

Keywords: Aflatoxin M_1; anti-idiotypic nanobody; chronoamperometry; milk; screen-printed carbon electrodes

1. Introduction

Aflatoxins are a class of *Aspergillus* fungal metabolites, among which aflatoxin B_1 is the most concerned mycotoxin due to its strong teratogenicity, carcinogenicity, and mutagenicity (Li, Liu, Zhang, Luo, Lin, & Jiang, 2021). AFM_1 is a product of the hydroxylated metabolism of aflatoxin B_1, which has mutagenic and teratogenic effects on humans, particularly infants. The World Health Organization and the International Agency for Research on Cancer classified AFM_1 as Group 2B human carcinogen (Du, Su, Yang, Pan, Liu, Gong, et al., 2016). AFM_1 is the major type of contaminant in milk and milk products. Thus, the safety related to milk consumption has gained immense attention worldwide. On account of the high toxicity of aflatoxins, strict limits were set by most countries worldwide. For example, Europe set a limit of 0.25 ng/mL for AFM_1 in milk, while the US Food and Drug Administration has set the maximum level for AFM_1 at 0.5 ng/mL in milk. It is rather essential to develop rapid detection methods for protecting consumption safety so as to detect the ultra-trace-level contamination in food as early as possible.

In recent years, competitive immunoassay has been widely employed for the rapid detection of mycotoxins(Lai, Wei, Xu, Zhuang, & Tang, 2017; Lin, Zhou, & Tang, 2017; Lin, Zhou, Tang, Niessner, & Knopp, 2017; Lin, Zhou, Tang, Niessner, Yang, & Knopp, 2016; Zhou & Tang, 2020). Immunosensors are used in AFM_1 measurements by incorporating enzyme catalysis (Di Giovanni, Zambrini, Varriale, & D'Auria, 2019), chromatography (Han, Gong, Wang, Zhang, Jin, Zhao, et al., 2019), electrochemistry (Abera, Falco, Ibba, Cantarella, Petti, & Lugli, 2019), and so forth. Most of them provide satisfactory detection results. Immunosensors based on electrochemistry can be a good way to detect AFM_1 due to their many advantages including cost- and time-effective procedure, sensitivity, and so forth (Jia, Liao, Fang, Jia, Liu, Li, et al., 2021; Wei, Sun, Gao, Yang, Ye, Ji, et al., 2021). In addition, immunosensors can be integrated with different types of detection strategies, especially low-cost devices such as SPCEs, which can be an excellent advantage for

mycotoxin detection. Compared with the traditional rod-type electrodes, SPCE technology offers remarkable benefits but is not limited to disposability and portability (Sharma, Istamboulie, Hayat, Catanante, Bhand, & Marty, 2017). As we know, recognition elements (monoclonal antibody, single-chain antibody, nanobody, aptamer, etc.) always decide the sensitivity and the limit of detection of immunosensors. Thus, research works have been done on developing high-quality antibodies to increase the sensitivity and feasibility of immunosensors.

Nanobody is a variable domain of heavy chain of heavy-chain antibody (VHH) obtaining from Camelidae species and sharks. VHH emerges as a nanobody because its molecular size is only about 15 kDa and the dimension is about $2.5 \times 3 \times 4$ nm^3 (Yu, Xu, Wu, Jiang, Wei, Zulipikaer, et al., 2020). The advantages of nanobodies include high affinity, selectivity, solubility, and yield and low-cost productions (Tang, Li, Zhang, Zhang, Zhang, & Jiang, 2017). Due to another disulfide bond in the complementary determining region 3, nanobodies exhibit high tolerance to organic solvents and high temperatures (Simões, Guedens, Keene, Kubiak-Ossowska, Mulheran, Kotowska, et al., 2021). AIdnb are developed by immunizing alpacas with monoclonal antibodies; they have “mirror image” relationships with the targets. With their favorable properties, AIdnb are considered as promising reagents that can replace highly toxic traditional antigens and standard solutions. Previous studies used AIdnb in enzyme-linked immunosorbent assay (ELISA), polymerase chain reaction (PCR), and immunochromatography successfully (Table S1). However, the field of application of AIdnb should be continuously expanded.

A screen-printed electrochemical immunosensor based on an alternative antigen was developed in this study to explore a new platform technique of AIdnb. This was the first assay established using a nontoxic SPCE electrochemical. It could perform the rapid, low-cost monitoring of milk consumption safety.

2. Experimental

2.1 Chemicals and reagents

Anti-aflatoxin M_1 monoclonal antibody (mAb) 2C9 was developed in our laboratory, which had cross-reaction with AFB_1, AFB_2, AFG_1, and AFG_2 of <0.01%. Aflatoxin B_1, B_2, G_1, G_2, M_1 standard, bovine serum albumin (BSA), isopropyl β-D-thiogalactopyranoside (IPTG), and 3, 3', 5, 5'-tetramethylbenzidine (TMB) were obtained from Sigma (MO, USA). A LeukoLOCK total RNA isolation system was obtained from Applied Biosystems (CA, USA). *Escherichia coli ER 2738* competent cells from the ER2673 line of *E. coli* were purchased from Lucigen Corp. (WI, USA). TOP10F' competent cells were procured from Life Technologies (NY, USA). Helper phage M13KO7, sfiI, and T4 DNA ligase were obtained from New England Biolabs (MA, USA). QIAprep Spin MinPrep Kit, QIAquick Gel Extraction Kit, and QIAquick PCR Purification Kit were obtained from Qiagen. Tween 20 was obtained from J&K Scientific (Beijing, China). Mouse anti-M13 monoclonal antibody conjugated to horseradish peroxidase (HRP) was purchased from Sino Biological (Beijing, China). Goat anti-mouse monoclonal antibody conjugated to HRP was purchased from Solarbio (Beijing, China). The Costar 96-well EIA/RIA plate was purchased from Corning Incorporated (Corning, NY, USA). Potassium ferrocyanide [$K_4Fe(CN)_6$], potassium ferricyanide [$K_3Fe(CN)_6$], BSA, N-hydroxysuccinimide (NHS), 1-ethyl-3-(3-dimethylamino-propyl)-carbodiimide (EDC), sodium phosphate dibasic (Na_2HPO_4), potassium phosphate monobasic (KH_2PO_4), magnesium chloride ($MgCl_2$), potassium chloride (KCl), sulfuric acid (98%), sodium chloride (NaCl), ethanol (98%), sodium nitrite ($NaNO_2$), 4-aminobenzoic acid, ethanolamine, HRP-conjugated secondary antibody and aflatoxin M_1 were purchased from Sigma–Aldrich (France). Ultrapure water from a Milli-Q system was used for preparing aqueous solutions and rinsing procedures.

2.2 Apparatus and electrodes

SPCEs, which consisted of three-electrode configurations (working, counter, and reference electrodes), were fabricated using a DEK 248 screen-printing system (BAE laboratory, Perpignan, France). Electrochemical measurements were performed on an Autolab PGSTAT100 potentiostat/galvanostat station equipped with a Nova 2.1 analyzer system (Metrohm Autolab B.V., Kanaalweg, The Netherlands).

2.3 Chemical modification of SPCEs

SPCEs were cleaned by applying six potential cycles between 1.5 to –1.0 V/pseudo Ag reference electrode with 100 mVs^{-1} scan rate in the mixture of 0.5 mol/L sulfuric acid and 0.1 mol/L KCl until clean SPCEs were obtained. The clean SPCEs were chemically modified according to the reactions shown in Scheme 1. As shown in Scheme 1a, the SPCEs were modified using 2 mmol/L sodium nitrite and 2 mmol/L 4-aminobenzoic acid (ABA) in 0.5 mol/L HCl. The mixture was allowed to react for 5 min for the maximum generation of diazonium salt at 4℃. Then, 150 µL of the salt solution was electrografted on SPCE to generate 4-carboxyphenyl diazonium salt SPCE (4-CP/SPCE) via linear sweep voltammetry (LSV) (potential: 0.4 V to –0.8 V; scan rate: 50 mVs^{-1}). The 4-CP/SPCEs were rinsed with phosphate-buffered saline (PBS) (0.01 mol/L) in the subsequent step.

The other modification method (Scheme 1b) involved preparing the 4-aminophenyl diazonium salt SPCE (4-AP/SPCE). The clean SPCEs were modified by the following procedure. In brief, 4 µL of 0.1 mol/L $NaNO_2$ was added to 196 µL of 2 mmol/L 4-nitroanilineaminobenzoic acid in 0.5 mol/L HCl, stirred, and reacted for 5 min at 4°C. Then, the 4-AP/SPCEs were generated by LSV from 0.4 to –0.5 V. The 4-AP/SPCEs were rinsed with PBS (0.01 mol/L) and used for the subsequent step.

Scheme 1

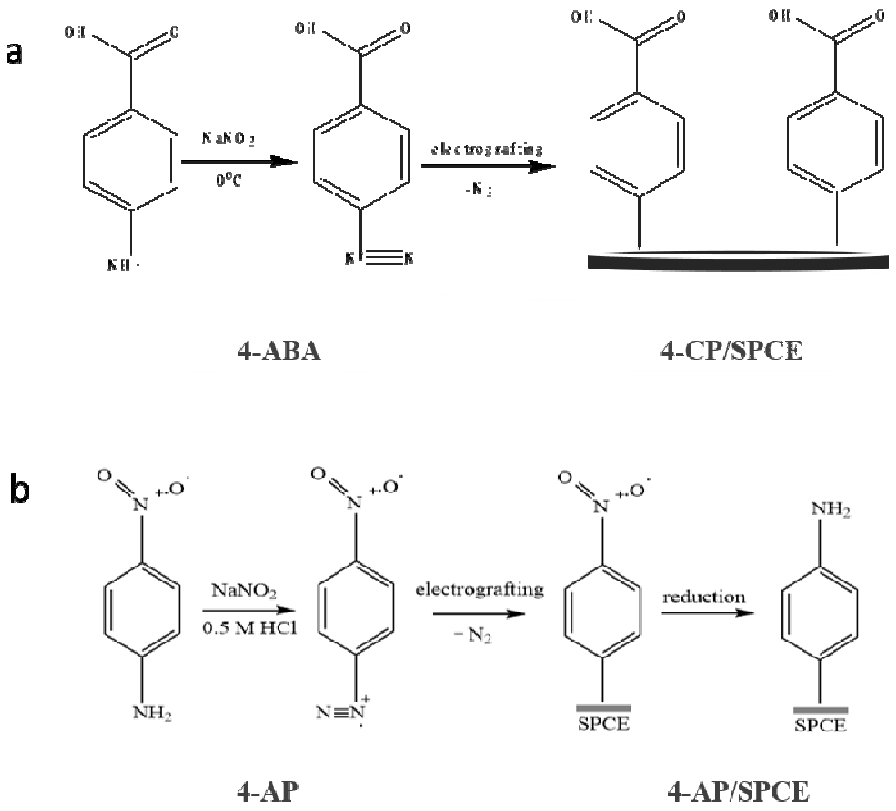

Scheme 1. Modification of SPCE with 4-aminobenzoic acid (a) and 4-aminophenyl diazonium salt (b).

2.4 Development of anti-idiotypic nanobody of AFM_1

The nanobody with a His tag at its C-terminal end was developed as depicted earlier. Briefly, a 2-year-old male alpaca was immunized with 100 μg/mL monoclonal antibody against AFM_1 (2C9). Total RNA was extracted and transcribed into cDNA. Primers were used to amplify the VHH and then ligated to the pComb3X. The pComb3X/VHH were transformed into *E. coli* ER 2738. The positive clones were screened by a completive elution method. During elution, 500, 20, and 5 ng/mL of aflatoxin M_1 in 10% methanol–PBS was used as the elution buffer for each round. Phagemids of positive clones were transformed into nonsuppressor *E. coli* strain TOP10F′ cells, expressed, and purified with Ni-NTA metal affinity chromatography. Finally, the nanobody was stored at –20℃ to use.

2.5 Immunosensor for detection of AFM_1

The principle of the immunosensor was based on the competitive reaction on SPCE. In the negative samples, the mAbs were captured by the nanobody on the working electrode surface while in the positive samples, the mAbs reacted with the AFM_1 resulting in less mAbs captured on the working electrode surface, the electrochemical signal decreased as a result of increased concentration of AFM_1. The assembly steps of the AFM_1 immunosensor and detection mechanism are illustrated in Scheme 2. Firstly, the modified SPCEs were activated by incubation with 20 μL of EDC/NHS/nanobody in 4 mg/mL N- methyl piperidine（MES）buffer (pH 6.8) for 180 min. After incubation, SPCEs were rinsed with PBS (0.01 mol/L, pH 7.4) and stored at 4℃ for further use. The competition step was performed by incubating antibody 2C9 and equivalent volumes from a series of concentrations of AFM_1 on the working electrode surface for 30 min at 37℃, with shaking at 250 rpm. The surface was rinsed six times with PBST (PBS containing 0.05% Tween 20). Subsequently, 15 μL of HRP-labeled secondary antibody was added to the working electrode surface, incubated for another 30 min, and rinsed six times with PBST. Then, 50 μL of TMB solution was used to cover the working counter and reference electrodes. The enzyme activity was measured electrochemically using chronoamperometry (CV).

Scheme 2

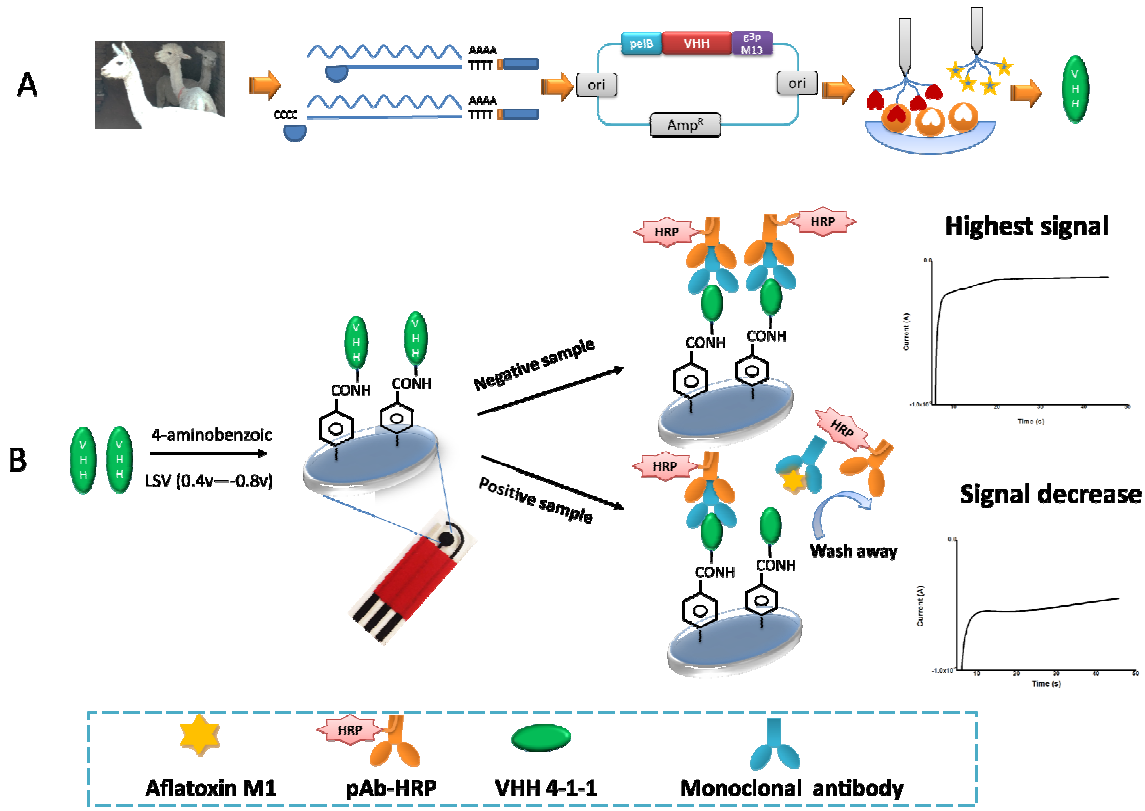

Scheme 2. (A) Development of nanobody VHH 4-1-1. (B) Fabrication process mechanism of a nanobody-based electrochemical immunosensor for AFM_1 detection.

2.6 Electrochemical measurements

The impedimetric measurements (electrochemical impedance spectroscopy, EIS) were used for characterizing the immunosensor surface using 1mM ferri/ferrocyanide/PBS ($[Fe(CN)_6]^{4-/3-}$/PBS) with a frequency range of 10 kHz to 0.5 Hz. The Nyquist plots were recorded with a cyclic voltammetry amplitude of 5 mV and a sampling rate of 20 points. The surfaces of SPCEs were characterized using EIS after each modification step. Chronoamperometry measurements were performed for 40 s at 0.4 V. Cyclic voltammetry measurements were obtained between maximum and minimum voltages of 0.8 V and –0.6 V (vs Ag/AgCl reference electrode), respectively, at a scan rate of 0.1 V/s.

2.7 Application of the immunosensor for real sample analysis

The milk sample was spiked with different concentrations of AFM_1 of 0, 0.25, 0.5, 1.25, 2.5, and 5.0 ng/mL. The milk samples were cultured at 40°C for 30 min and then demulsified with ethanol (1/3, *v*/*v*). Further, 800 μL of milk was centrifuged at 6000 rpm for 5 min, followed by adding 90.0 μL of PBS to 10.0 μL of supernatant. Based on the optimized parameter detection, the current signal value corresponding to each concentration was determined. By calculating the ratio between different concentrations of AFM_1 and the blank one (without AFM_1 standard), the standard curve between the ratio and the corresponding AFM_1 concentration was established.

3. Results and Discussion

3.1 Nanobody characterization

The total RNA was extracted from the blood of immunized alpaca, and then the heavy-chain IgG2 and IgG3 sequences were amplified (Fig. S1), followed by the insertion of the amplified sequence into the vector pComb 3X. The constructed nanobody library exhibited a size of 2.7×10^7 (Fig. S2). We utilized a competitive panning strategy to select the specific nanobody. After three rounds of panning, two sequences were obtained, defined as VHH 4-1-1 and VHH 2-3-1. Both contained 37 F, 38 R, 40 F, 42 G, 45 R, and 46 E in FR2, which explained the solubility of nanobodies (Fig.1A). The two plasmids were transformed to TOP10F` for expression, and the nanobody with 6× His tag was purified using an Ni-NTA affinity column (Fig.1C). The nanobodies were tested for their sensitivity and specificity by indirect competitive ELISA. The IC50 of nanobodies against AFM_1 and 2C9 was 8.54 and 3.33 ng/mL, respectively. The cross-reactivity of VHH 4-1-1 and VHH 2-3-1 with other mAbs against AFM_1 (2C9, 13# and 47#) was 100%, <0.1%, and 17.7% and 100%, <0.1%, and <0.1%, respectively (Fig.1B). The stability of nanobody was investigated. The results showed that the gene sequence of VHH 2-3-1 changed during subculture, the 5 V changed to 5 A, and 86 K changed to 86 N. Therefore, VHH 4-1-1 was selected as the recognition reagent to establish the detection method.

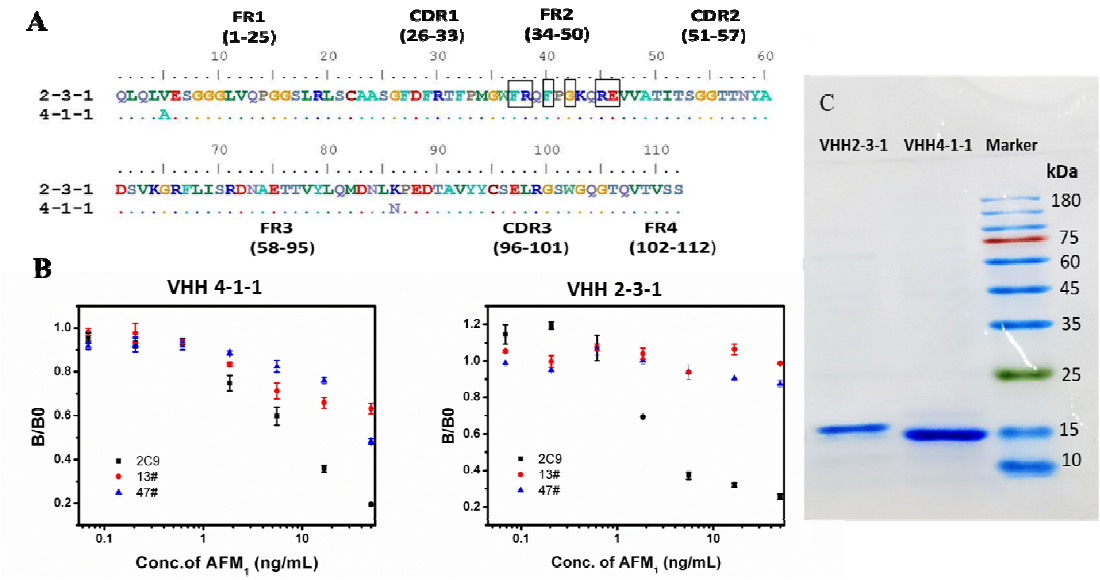

Figure 1. Nanobody selection and characterization. (A) Two classes of nanobodies containing different amino acid sequences were determined, named VHH 2-3-1 and VHH 4-1-1. (B) Cross-reactivity of nanobodies with mAb 2C9, 13# and 47#. (C) VHH 2-3-1 and VHH 4-1-1 were purified and analyzed by SDS-PAGE.

3.2 Characterization of the immunosensor for AFM_1

3.2.1 Modification of SPCEs

In the classical immunoassay, the antibody/antigen should immobilized on the solid phase to ensure immune reaction succesfully. Two nanobody modification methods, 4-aminobenzoic acid SPCE (SPCE-4ABA) with -COOH and 4-aminophenyl diazonium salt SPCE (SPCE-AP) with –NH, were compared to ensure that the active sites of nanobodies were exposed to the antibody. The results showed that using the SPCE-4ABA modification, the current signal decreased with the increase in AFM_1 standard solution, while no signal changed using SPCE-AP modification. The N-terminal covalent coupling with the functional SPCE-4ABA yielded better results. Previous studies have shown that localized and oriented immobilization of antibodies could avoid interference with the structure and function of antibodies (Sivaram, Wardiana, Howard, Mahler, & Thurecht, 2018). In this study, we concluded that using functional SPCE-4ABA, the epitope of nanobody was almost fully exposed to ensure

maximum binding with the antibody. On the contrary, using functional SPCE-AP, the epitope of nanobody was hidden by itself or SPCE, and it was difficult to capture the antibody effectively.

3.2.2 Electrochemical characterization

EIS offers detailed data of surface change after each modification step of the SPCE electrode. Figure 2A shows the semicircle portion of SPCE, which responded to the electron-transfer resistance. The bare SPCE exhibited the smallest semicircle, which had a low electron-transfer resistance. After diazotization of the SPCE electrode surface with 4-ABA and $NaNO_2$, the semicircle increased obviously, revealing that the deposition of the negative terminal on the SPCE surface led to an increase in electron-transfer resistance. The Nb-SPCE activated with EDC/NHS induced a decrease in the semicircle ascribed to the replacement of the carboxyl group by the nanobody, leading to the decrease in electron-transfer resistance. After modifying the mAb, the semicircle increase was attributed to the blocking behavior of mAb, which hindered the diffusion of the redox probe. The results of EIS confirmed the successful modification of the SPCE. LSV and CV were provided to identify the successful modification of SPCE. As shown in Figure S3, a significant signal peak was observed, implying that the diazonium salt was reduced on the SPCE. The bare SPCE and SPCE-4ABA were detected using CV scanning to further verify whether benzoic acid was modified to the surface of SPCE successfully. As shown in Figure S4, the results showed a pair of reversible redox peaks in the bare SPCE scanning curve: EPA = +0.5542 V; EPC = –0.21973V; and the difference between the oxidation peak and the reduction peak $\Delta EP = 0.774$ V, corresponding to the redox reaction of $[Fe(CN)_6]^{4-/3-}$. The redox peak current of SPCE-4ABA was significantly lower than that of the bare SPCE because the benzoic acid modified on the SPCE hindered the electron transfer of $[Fe(CN)_6]^{4-/3-}$ (Fig. S4).

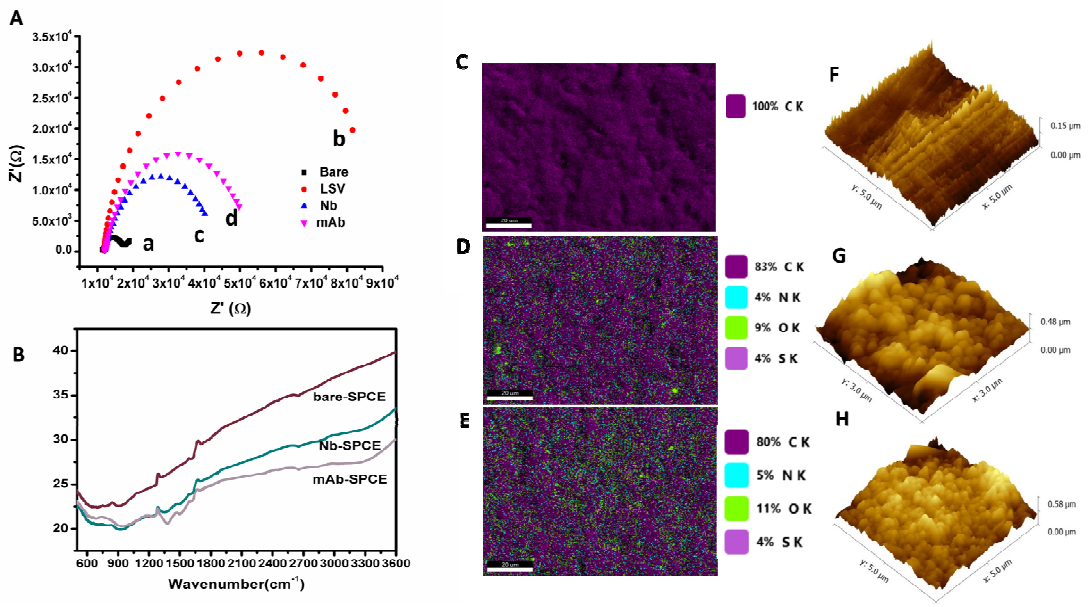

Figure 2. (A) Nyquist plots of modified SPCEs detected with 1mM $Fe(CN)_6]^{4-/3-}$/PBS. (a) Bare SPCE, (b) SPCE-4ABA, (c) Nb-SPCE, and (d) mAb-SPCE. (B) FT-IR characterization of bare SPCE, Nb-SPCE, and mAb-SPCE. (C) TEM mapping of bare SPCE, (D) Nb-SPCE, and (E) mAb-SPCE. (F) AFM image of bare SPCE, (G) Nb-SPCE, and (H) mAb-SPCE.

3.2.3 FT-IR, TEM mapping, and AFM characterization

FT-IR, SEM, and atomic force microscopy (AFM) were performed for the characterization of bare SPCEs, nanobody modification SPCEs (Nb-SPCEs), and mAb modification SPCEs (mAb-SPCEs).

The results of the FT-IR spectrum confirmed that the Nb-SPCEs had absorption bands at 1229–1301 cm^{-1} and vibration bands at 3300 cm^{-1} (str.,-NH), which revealed the presence of nanobody after coupling conjugation. Then, after incubation with mAb, much clear absorption bands were observed at amide III (1229–1301cm^{-1}) and 3300 cm^{-1}, which strongly confirmed the mAb binding with the nanobody (Fig. 2B). Transmission electron microscopy (TEM) mapping was used to characterize elemental distribution on the working electrode of SPCEs. Figure 2C shows 100% elemental C located on the working electrode of bare SPCE. Figure 2D and 2E represents the appearance of new elemental, including N, O, and S located on the surface of the electrode, indicating that the nanobody and mAb were conjugated on the surface of SPCE successfully. AFM is a surface analysis technique capable of

imaging the topographical and morphological changes in a specimen surface. The AFM topographies of Nb-SPCEs showed an overlap of proteins and a uniform surface compared with the bare SPCEs (Fig. 2F and 2G), indicating that the nanobody was modified on the working electrode successfully. After incubating mAb, the surface morphology of SPCE was changed due to the nanobody and antibody recognition mechanism, the surface of working electrode overlap protein and becoming uniform further (Fig.2H).

3.3 Experimental parameter optimization

The important parameters, including concentrations of nanobody, mAb, and HRP-IgG, required time for incubation, and blocking method, were studied to obtain the most sensitive and effective analytical performance of immunosensors for AFM_1 detection. All the parameters were optimized by measuring the different absolute values of the current signal. The larger the difference, the higher the sensitivity of the analysis, which meant the higher the binding rate of the antibody. The different absolute values of the current signal were estimated directly using the following formula:

$$\Delta Current = |Current_{blank}| - |Current_{AFM1}|$$

where $Current_{blank}$ is the current response value of mAb 2C9 and PBS incubated; $Current_{AFM1}$ is the current response value of mAb 2C9 and AFM_1 incubated.

3.3.1 Nanobody and antibody concentration

The amounts of antigens and antibodies were considered as the key factors in developing immunoassay methods. In theory, the lower the antigen concentration used in the competitive reaction, the higher the sensitivity. Different concentrations of 4.375, 8.75, and 17.5 μg/mL of VHH 4-1-1 used as surrogate antigens were immobilized on the working electrode. As observed in Figure 3A, the value of the ΔCurrent was directly proportional to the VHH4-1-1 concentration until 17.5 μg/mL. The optimization of mAb 2C9 was carried out using different concentrations of 0.50,

0.33, and 0.25 μg/mL. The maximum value of the ΔCurrent was obtained at 0.33 μg/mL, which then decreased at higher concentrations, indicating that the more amounts of mAb 2C9 needed much more free targets to match with, leading to a decrease in sensitivity on AFM_1 analysis (Fig. 3B). The best concentration of HRP-IgG was used at 1:5000 dilution (Fig. 3D).

3.3.2 Blocking method and immunoreaction time optimization

In a traditional immunoassay, it is necessary to block any remaining active sites of AFM_1; otherwise, it is considered that the incomplete blockage will affect the accuracy of the immunosensor. Therefore, the effect of the blocking method on the detection sensitivity was investigated. Two blocking buffers, 0.1 mol/L ethanolamine/Tris HCl (pH 7.4) and 1% BSA/PBS (*w*/*v*) were compared with the control group having no blocking. The ΔCurrent of both blocking methods did not show any obvious change with the AFM_1 increase, considering that ethanolamine blocked the whole active sites, including the sites of the nanobody reacting with the mAbs. The molecule of BSA was too big and blocked all the binding active sites of the nanobody. Therefore, the working electrode was without any blocking in this experiment (Fig. 3E).

With the other factors fixed, the optimization of the immunoreaction time was performed using the immunosensor (nanobody concentration of 0.33 μg/mL; mAb 2C9 concentration of 17.5 μg/mL; HRP-IgG 1:5000 dilution) with AFM_1 at a concentration of 10 ng/mL for different time durations. The results showed that the inhibition rate reached the maximum when the incubation time was 30 min, indicating that much higher amounts of AFM_1 were needed to match with the mAb after that time (Fig. 3F).

3.3.3 Substrate optimization

Finally, the substrate is another critical factor that provides an amplification electrochemistry signal of the immunoreaction. The efficiency of the substrates, hydroquinone, and TMB was evaluated by the CA analysis of the HRP enzyme

activities. The results in Fig. 3C demonstrated the TMB radical cation and the charge-transfer complex of the diamine and the diamine were formed in the first step. Then, the intermediate product was further electro-oxidized to the complete oxidation product quinone diimine in the second step. Since the oxidation peak located at 0.07 V was considered that of the final products of TMB (TMB^{2+}), the second peak current was used as the optimal applied potential of TMB in the following experiment(Jin, Ko, Kim, Tran, Son, Geng, et al., 2018). The optimal applied potential of hydroquinone was –0.271 V, as assayed by CV. The use of hydrogen peroxide and benzoquinone resulted in no differences in the ΔCurrent value, while TMB and H_2O_2 yielded a ΔCurrent value of 3.69×10^{-7} (Fig. 4A, B). The absolute value of the current signal collected in 30 s decreased, which was consistent with the results of competitive detection in theory; that is, the higher the concentration of the target, the lower the signal value. Therefore, HRP was used to catalyze the H_2O_2 oxidation of TMB for electrochemical signal reaction.

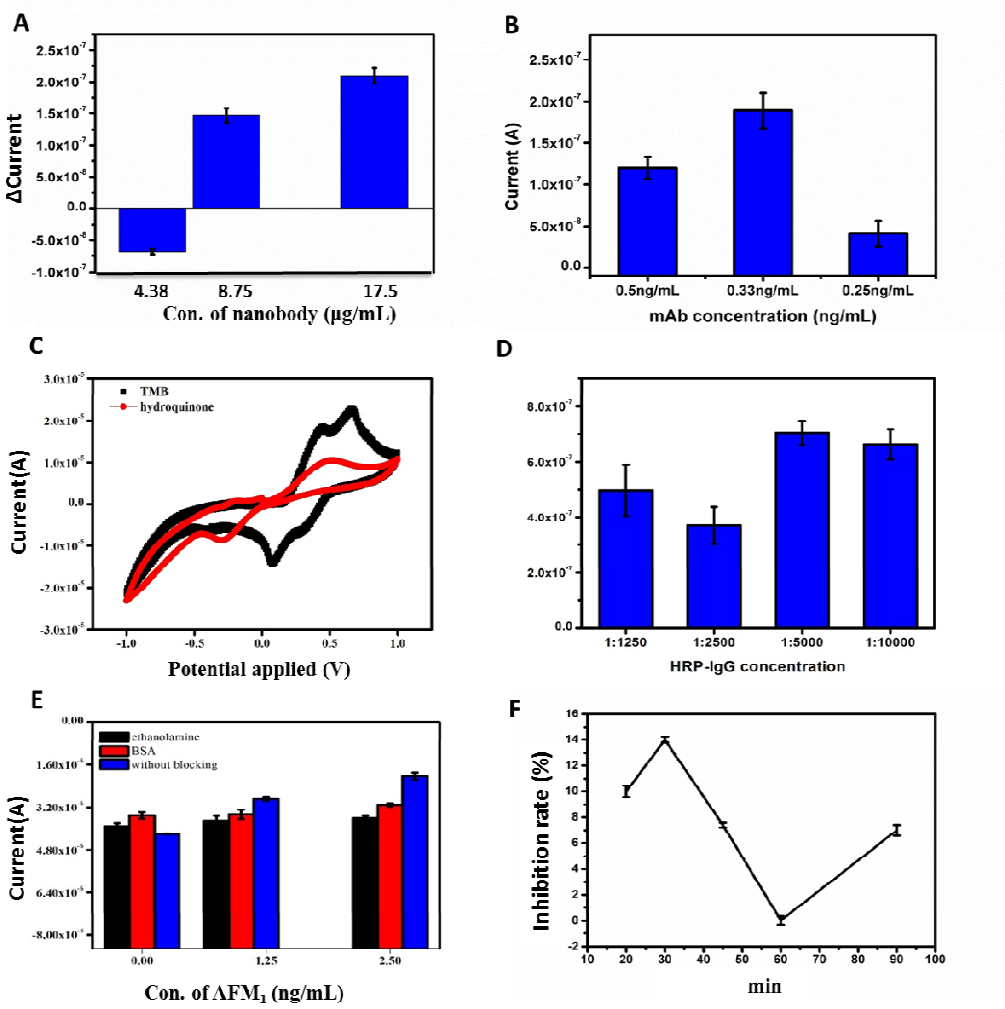

Figure 3. Currents values *via* CV on (A) nanobody concentration, (B) mAb concentration, (C) substrate reagents, (D) HRP-IgG concentration, (E) blocking methods, and (F) incubation time of samples.

3.4 Detection of AFM_1

With the optimization of the aforementioned factors, the immunosensor was incubated with different concentrations of AFM_1 to establish the standard curve. As shown in Figure 4C, a linear relation between the current responses and the logarithm of the AFM_1 concentration was observed in the range 0.25–5.0 ng/mL, which could be fitted into a linear regression equation: y = –2E-06x + 4E-06, R = 0.9981, where y is the value of current, and x is the Log of AFM_1 concentration. In the blank sample (without AFM_1), the HRP enzyme concentration is high and the redox reaction rate is fast, resulting in the faster current, so the absolute value of current is large. With the AFM_1 concentration increase in the sample, the HRP concentration decrease and the

reaction speed decrease, resulting in the slower current, so the absolute value of current is smaller. The developed immunosensor demonstrated a sensitivity toward AFM_1 with a detection limit at 0.09 ng/mL, which was calculated using 3SD of blank samples. The sensitivity of the assembled immunosensor could meet the requirement of the maximum residual levels in most countries, such as China, the EU, and so forth. Especially the SPCEs were low cost and could be easily applied in developing countries. There were other immunoassays using different kinds of electrodes for AFM_1 detection. For example, Guo et al. constructed a covalent organic frameworks TpBD on glassy carbon electrode using paminobenzoic acid and ethylenediamine as connector, the developed electrochemical biosensor exhibited high selectivity and sensitivity toward AFM_1 with a LOD of 0.15 ng/mL(Guo, Wang, Pang, Shen, Yang, Ma, et al., 2021). Karczmarczyk et al. developed a strategy based on a competitive immunoassay for the voltammetric detection of mycotoxins (OTA and AFM_1) using modified gold screen printed electrodes with IC80 of 0.04 ng/mL for AFM_1(Karczmarczyk, Baeumner, & Feller, 2017). Li et al. developed an inner filter effect-based immunosensor incorporating fluorescent detection for AFM_1 residue analysis with a LOD of 18.10 ng/kg (Li, Liu, Zhang, Luo, Lin, & Jiang, 2021). All the established methods above obtained satisfied results, performing based on the traditional antigens and antibodies reaction. In our work, the AIdnb were used to replace the high toxin traditional antigens to modify the surface of working electrode. In conclusion, compared with other kinds of electrodes, the SPCE used in this work are not only modified with non-toxic alternative antigens to meet the needs of environmental friendly, but also have high sensitivity. Moreover, SPCE has the advantages of convenient use and low-cost, and has broad application prospects in food safty detection.

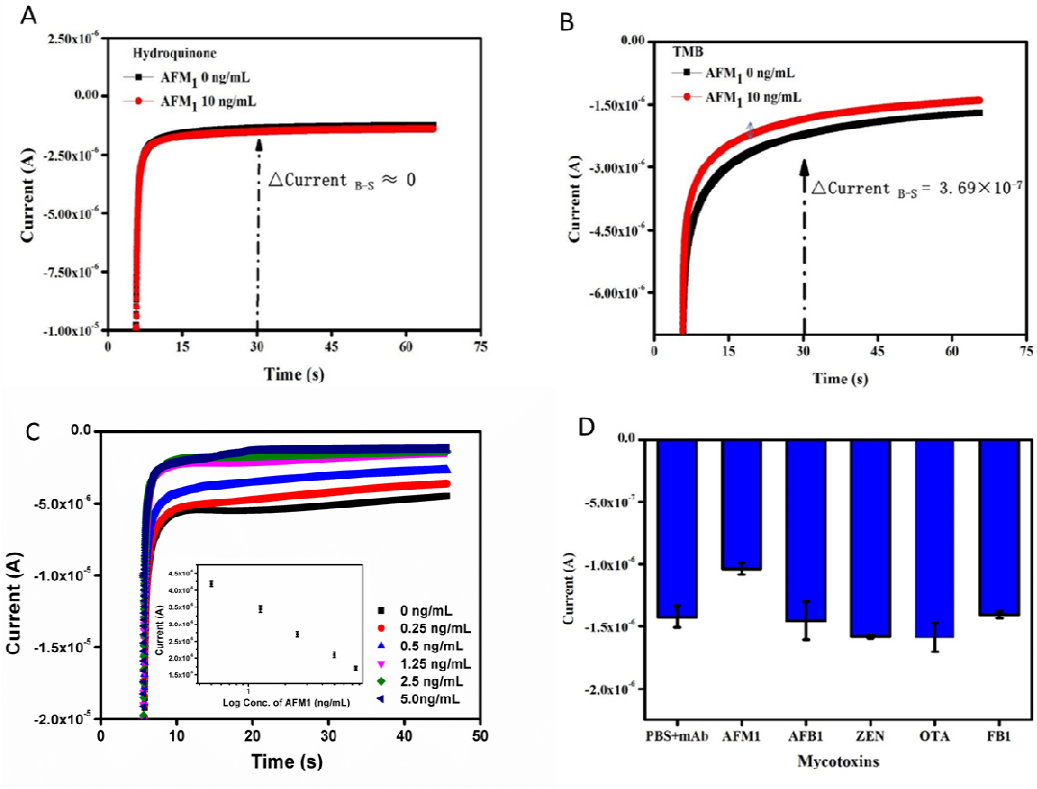

Figure 4. (A) Electrocatalytic current response of the immunosensor for the detection of AFM_1 at 0 ng/mL and 10 ng/mL using hydroquinone and (B) TMB; (C) Current response of immunosensor for the detection of AFM_1 (ng/mL): (a) 0, (b) 2.5, (c) 0.5, (d) 1.25, (e) 2.5, and (f) 5.0 ng/mL. The inset represents the linear curve of the immunosensor obtained for AFM_1 concentrations. (D) Electrocatalytic current response of the immunosensor for detecting AFM_1, AFB_1, ZEN, OTA, and FB_1 at a concentration of 10 ng/mL. The error bars were obtained from five parallel experiments.

3.5 Specificity, stability, and validation of the immunosensor

The specificity of the proposed immunosensor was investigated by measuring the current responses to AFB_1, ZEN, OTA, and FB_1 at a concentration of 10 ng/mL. The current response exhibited no decrease compared with the blank (PBS), indicating that the immunosensor had satisfactory specificity without nonspecific reaction with AFB_1, ZEN, OTA, and FB_1 (Fig. 4D). The electrode stability of the immunosensor was investigated by detecting the influence of electrode storage time on the current response value. After incubating the nanobody on the electrode, the same patch electrode was stored in the dark for different periods before detecting the blank

sample and the sample spiked with 10 ng/mL of AFM_1. It exhibited that 95% of the initial current signal was retained after storage at 4°C for 9 weeks, indicating that the immunosensor had good stability. Compared with the monoclonal antibody, nanobody exhibit thermal stability and showed better tolerance to organic solvents (He, Nie, Yan, Zhu, He, Li, et al., 2022; He, Wang, Li, Zhang, Lei, Zhang, et al., 2014). Thus, in theoretically, the nanobody modified electrode can be regenerated. However, the actual regeneration results should be proved by experimental data further.

We examined the performance of the immunosensor at different concentrations of AFM_1 (0.25, 0.5, and 1.0 ng/mL); the recoveries of the assays were 82.0%–108.0% (Table 1). We detected the intra-assay variability on the same day and the inter-assay variability on different days with the immunosensor to study the stability of the immunosensor. The intra-assay variability was given by the average of five replicated SPCEs. The inter-assay was given by the average of five replicated SPCEs on different days. The relative standard deviation was 10.1%–11.5% for intra-assays and 10.2%–13.0% for inter-assays, which showed that it was feasible to determine AFM_1 using the immunosensor.

Table 1. Recovery analysis of the immunosensor for AFM_1 in milk samples

	Spiked concentration (ng/mL)	Mean±SD (ng/mL)	Recovery (%)	RSD (%)
Intraday (n=5)	0.25	0.27	108.0	10.6
	0.5	0.41	82.0	11.5
	1.0	0.85	85.0	10.1
Interday (n=5)	0.25	0.26	104.0	12.6
	0.5	0.43	86.0	10.2
	1.0	0.83	83.0	13.0

Furthermore, 10 naturally contaminated milk samples collected from local farms were detected using the immunosensor and high performance liquid chromatography-mass spectrometry (HPLC-MS/MS). The results obtained from the analysis are summarized in Table 2. A total of 4 samples (40% of 10 samples) were found to contain AFM_1

with a concentration of lower than 0.47 ng/mL. The results showed a satisfactory agreement between the immunosensor and HPLC-MS/MS, indicating that the proposed method was highly appropriate for the screening and quantitation of AFM_1 in milk.

Table 2. Validation of the immunosensor by HPLC-MS/MS for AFM_1 in natural milk samples

Sample	HPLC-MS/MS (n=5) Mean (ng/mL)	Immunosensor (n=5) Mean (ng/mL)
1	ND[a]	ND
2	0.40±0.001	0.43±0.56
3	ND	ND
4	0.46±0.005	0.47±0.72
5	ND	ND
6	0.38±0.004	0.40±0.51
7	ND	ND
8	ND	ND
9	0.26±0.008	0.28±0.69
10	ND	ND

[a]ND: not detected.

4. Conclusions

In summary, a nontoxic electrochemical immunosensor was developed based on novel anti-idiotypic nanobody-functionalized SPCEs, and applied to identify AFM_1 using the immunosensor. Due to the specificity and stability of the nanobody, the proposed immunosensor exhibited excellent analytical performance with a linear range (0.25–5.0 ng/mL), as well as a low limit of detection value (0.09 ng/mL), meeting the requirement of the regulatory standard. In addition, the immunosensor showed

475 excellent recovery (%) in samples, proving that the immunosensor had high accuracy
476 and repeatability for the quantitative determination of AFM_1 by chronoamperometry.
477 The proposed immunosensor could be further used in the naturally contaminated
478 samples for AFM_1 detection.
479

Reference

Abera, B. D., Falco, A., Ibba, P., Cantarella, G., Petti, L., & Lugli, P. (2019). Development of Flexible Dispense-Printed Electrochemical Immunosensor for Aflatoxin M1 Detection in Milk. *Sensors, 19*(18), 3912.

Di Giovanni, S., Zambrini, V., Varriale, A., & D'Auria, S. (2019). Sweet Sensor for the Detection of Aflatoxin M1 in Whole Milk. *ACS Omega, 4*(7), 12803-12807.

Du, B., Su, X., Yang, K., Pan, L., Liu, Q., Gong, L., Wang, P., Yang, J., & He, Y. (2016). Antibody-Free Colorimetric Detection of Total Aflatoxins in Rice Based on a Simple Two-Step Chromogenic Reaction. *Analytical Chemistry, 88*(7), 3775-3780.

Guo, L.-L., Wang, Y.-Y., Pang, Y.-H., Shen, X.-F., Yang, N.-C., Ma, Y., & Zhang, Y. (2021). In situ growth of covalent organic frameworks TpBD on electrode for electrochemical determination of aflatoxin M1. *Journal of Electroanalytical Chemistry, 881*, 114931.

Han, M., Gong, L., Wang, J., Zhang, X., Jin, Y., Zhao, R., Yang, C., He, L., Feng, X., & Chen, Y. (2019). An octuplex lateral flow immunoassay for rapid detection of antibiotic residues, aflatoxin M1 and melamine in milk. *Sensors and Actuators B: Chemical, 292*, 94-104.

He, T., Nie, Y., Yan, T., Zhu, J., He, X., Li, Y., Zhang, Q., Tang, X., Hu, R., Yang, Y., & Liu, M. (2022). Enhancing the detection sensitivity of nanobody against aflatoxin B1 through structure-guided modification. *Int J Biol Macromol, 194*, 188-197.

He, T., Wang, Y., Li, P., Zhang, Q., Lei, J., Zhang, Z., Ding, X., Zhou, H., & Zhang, W. (2014). Nanobody-based enzyme immunoassay for aflatoxin in agro-products with high tolerance to cosolvent methanol. *Anal Chem, 86*(17), 8873-8880.

Jia, M., Liao, X., Fang, L., Jia, B., Liu, M., Li, D., Zhou, L., & Kong, W. (2021). Recent advances on immunosensors for mycotoxins in foods and other commodities. *TrAC Trends in Analytical Chemistry, 136*, 116193.

Jin, G. H., Ko, E., Kim, M. K., Tran, V.-K., Son, S. E., Geng, Y., Hur, W., & Seong, G. H. (2018). Graphene oxide-gold nanozyme for highly sensitive electrochemical detection of hydrogen peroxide. *Sensors and Actuators B: Chemical, 274*, 201-209.

Karczmarczyk, A., Baeumner, A. J., & Feller, K.-H. (2017). Rapid and sensitive inhibition-based assay for the electrochemical detection of Ochratoxin A and Aflatoxin M1 in red wine and milk. *Electrochimica Acta, 243*, 82-89.

Lai, W., Wei, Q., Xu, M., Zhuang, J., & Tang, D. (2017). Enzyme-controlled dissolution of MnO2 nanoflakes with enzyme cascade amplification for colorimetric immunoassay. *Biosensors and Bioelectronics, 89*, 645-651.

Li, G., Liu, C., Zhang, X., Luo, P., Lin, G., & Jiang, W. (2021). Highly photoluminescent carbon dots-based immunosensors for ultrasensitive detection of aflatoxin M1 residues in milk. *Food Chemistry, 355*, 129443.

Lin, Y., Zhou, Q., & Tang, D. (2017). Dopamine-Loaded Liposomes for in-Situ Amplified Photoelectrochemical Immunoassay of AFB1 to Enhance Photocurrent of Mn2+-Doped Zn3(OH)2V2O7 Nanobelts. *Analytical Chemistry, 89*(21), 11803-11810.

Lin, Y., Zhou, Q., Tang, D., Niessner, R., & Knopp, D. (2017). Signal-On Photoelectrochemical Immunoassay for Aflatoxin B1 Based on Enzymatic Product-Etching MnO2 Nanosheets for Dissociation of Carbon Dots. *Analytical Chemistry, 89*(10), 5637-5645.

Lin, Y., Zhou, Q., Tang, D., Niessner, R., Yang, H., & Knopp, D. (2016). Silver Nanolabels-Assisted Ion-Exchange Reaction with CdTe Quantum Dots Mediated Exciton Trapping for Signal-On

Photoelectrochemical Immunoassay of Mycotoxins. *Analytical Chemistry, 88*(15), 7858-7866.

Sharma, A., Istamboulie, G., Hayat, A., Catanante, G., Bhand, S., & Marty, J. L. (2017). Disposable and portable aptamer functionalized impedimetric sensor for detection of kanamycin residue in milk sample. *Sensors and Actuators B: Chemical, 245*, 507-515.

Simões, B., Guedens, W. J., Keene, C., Kubiak-Ossowska, K., Mulheran, P., Kotowska, A. M., Scurr, D. J., Alexander, M. R., Broisat, A., Johnson, S., Muyldermans, S., Devoogdt, N., Adriaensens, P., & Mendes, P. M. (2021). Direct Immobilization of Engineered Nanobodies on Gold Sensors. *ACS Applied Materials & Interfaces, 13*(15), 17353-17360.

Sivaram, A. J., Wardiana, A., Howard, C. B., Mahler, S. M., & Thurecht, K. J. J. A. h. m. (2018). Recent advances in the generation of antibody–nanomaterial conjugates. *7*(1), 1700607.

Tang, X., Li, P., Zhang, Q., Zhang, Z., Zhang, W., & Jiang, J. (2017). Time-Resolved Fluorescence Immunochromatographic Assay Developed Using Two Idiotypic Nanobodies for Rapid, Quantitative, and Simultaneous Detection of Aflatoxin and Zearalenone in Maize and Its Products. *Analytical Chemistry, 89*(21), 11520-11528.

Wei, K., Sun, J., Gao, Q., Yang, X., Ye, Y., Ji, J., & Sun, X. (2021). 3D “honeycomb” cell/carbon nanofiber/gelatin methacryloyl (GelMA) modified screen-printed electrode for electrochemical assessment of the combined toxicity of deoxynivalenol family mycotoxins. *Bioelectrochemistry, 139*, 107743.

Yu, X., Xu, Q., Wu, Y., Jiang, H., Wei, W., Zulipikaer, A., Guo, Y., Jirimutu, & Chen, J. (2020). Nanobodies derived from Camelids represent versatile biomolecules for biomedical applications. *Biomaterials Science, 8*(13), 3559-3573.

Zhou, Q., & Tang, D. (2020). Recent advances in photoelectrochemical biosensors for analysis of mycotoxins in food. *TrAC Trends in Analytical Chemistry, 124*, 115814.

Declaration of competing interest

The authors declare that they have no known competing financial interests or personal relationships that could have appeared to influence the work reported in this paper.

Credit authorship contribution statement

Xiaoqian Tang: Conceptualization, Investigation, Formal analysis, Writing - original draft. **Gaëlle Catanante:** Supervision, Methodology. **Xiaorong Huang:** Validation. **Jean-Louis Marty:** Conceptualization, Visualization. **Qi Zhang:** Supervision, Formal analysis, Methodology. Supervision. **Hong Wang:** Validation, **Peiwu Li:** Project administration, Funding acquisition.